



Improved petrophysical characterization of Miocene deposits in south Tulamura anticline, India: An integrated geophysical and machine learning approach

PRADEEP KUMAR^{1,2}, SATYA NARAYAN^{1,*} , RAVINDRA MISHRA¹ and BIRENDRA PRATAP²

¹*Oil and Natural Gas Corporation Limited (ONGC), Dehradun 248 003, India.*

²*Institute of Science, Banaras Hindu University (BHU), Varanasi 221 003, India.*

**Corresponding author. e-mail: narayan_satya2@ongc.co.in satya.ismdhanbad@gmail.com*

MS received 30 October 2023; revised 16 February 2024; accepted 19 February 2024

With the high demand for fossil fuels, exploring the frontier areas for hydrocarbon reserves has become imperative. The recent discoveries in Gojalia, Sonamura, Baramura, and Sundalbari fields emphasize the need to explore additional anticlinal structures in Tripura for hydrocarbon exploration. Tulamura anticline (the study area) produced gas from Upper Bhuban, establishing hydrocarbon prospectivity in the northern part, but the southern part remains largely unexplored. An electro-log interpretation revealed the presence of sand facies deposited in a fining upward sequence, suggesting channel deposition. An integrated geophysical approach using seismic inversion and machine learning techniques was performed to delineate and characterize the litho-facies dispersal patterns in the Tulamura field. Spectral decomposition (12, 20 and 28 Hz) of stacked seismic data were RGB (red-green-blue) blended, revealing the southward striking channel geometry of the Bhuban Formation at a depth of 2220 m. The 3D P-impedance and V_p/V_s ratio volumes were estimated using the model-based pre-stack seismic inversion. Inversion results help discriminate among sand, shale and siltstone litho-facies. Petrophysical property (effective porosity) was predicted by combining the post-stack seismic attributes and well-log data using neural network modelling. The identified sand facies within the channel geometry exhibit relatively moderate to low P-impedance (9800–10600 m/s * gm/cm³), low V_p/V_s ratio (1.68–1.76), and moderately high effective porosity (8–13%) from surroundings, indicating favourable conditions for hydrocarbon accumulations. Shale between channels and major faults can create favourable stratigraphic entrapment, while an upward fining sequence suggests an intact top seal. This study advocates an integrated approach involving geophysical inversion and machine learning to identify optimal conditions for hydrocarbon accumulation within sand facies, supported by structural and stratigraphic entrapment.

Keywords. Reservoir characterization; machine learning; pre-stack inversion; petrophysical properties; Tripura–Cachar Fold Belt.

1. Introduction

India ranks third globally in oil/gas consumption, around 5 million barrels per day, with a yearly demand growth of 3–4%. Hydrocarbon exploration in India was initiated in the middle of the nineteenth century and geared up with commercial oil production in Assam in 1889. Since then, several fields in northeast India with proven oil/gas reserves have been explored. Previously, various geoscientists have applied many conventional geophysical methods to identify and delineate the responsible factors for hydrocarbon accumulations (Darijani *et al.* 2019; Narayan *et al.* 2022a, b, 2023b). However, these methods provide limited insights regarding the characteristics of the different litho-facies at depth (Biswas *et al.* 2014). In the recent past, several studies have demonstrated the successful application of inversion and machine learning algorithms integrating seismic and wireline log data to minimize the risk involved in hydrocarbon exploration (Kumar *et al.* 2016; Gogoi *et al.* 2018; Narayan *et al.* 2022a, b). Tulumura anticline is a linear, NNW–SSE trending, doubly plunging, asymmetric anticline, about 40 km long and 18 km wide at its widest part (figures 1 and 2).

The study area has experienced intense folding, faulting, and thrusting during post-collision orogeny (Murty 1983; Naik *et al.* 2001). In general, the thick clastic sequence of Tertiary sediments represents the stratigraphy of the study area. Based on the relative abundance of coarse and finer clastics presence, the Bhuban Formation (Early to Middle Miocene) was subdivided into three members such as Lower Bhuban, Middle Bhuban and Upper Bhuban (Evans 1932).

In the present study, we applied various cutting-edge geophysical and machine learning tools on high-resolution 3D seismic and well-log data to delineate and characterize the possible dispersal pattern of the hydrocarbon-containing sandstone facies in the study area. Spectrally decomposed seismic data was initially analyzed to bring out possible channel geometry. Then, the seismic inversion method was used to calculate the rock parameters to identify and characterize the lithofacies. The acoustic impedance and V_p/V_s ratio were estimated by performing pre-stack seismic inversion (Latimer *et al.* 2000). In general, acoustic impedance is a good indicator of lithology. In contrast, the V_p/V_s ratio indicates the presence of fluid types within the reservoir rock.

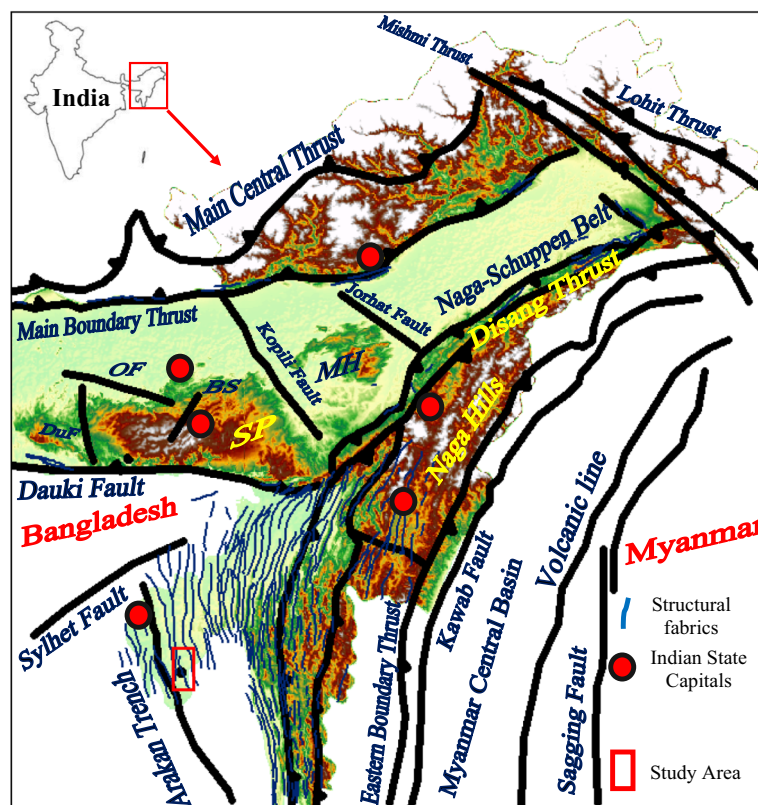


Figure 1. Tectonic map of northeast India. The study area (Tulumura field) is shown by the red rectangle. MH: Mikir Hill, SP: Shillong Plateau, DF: Dauki Fault and DuF: Dupitila Fault.

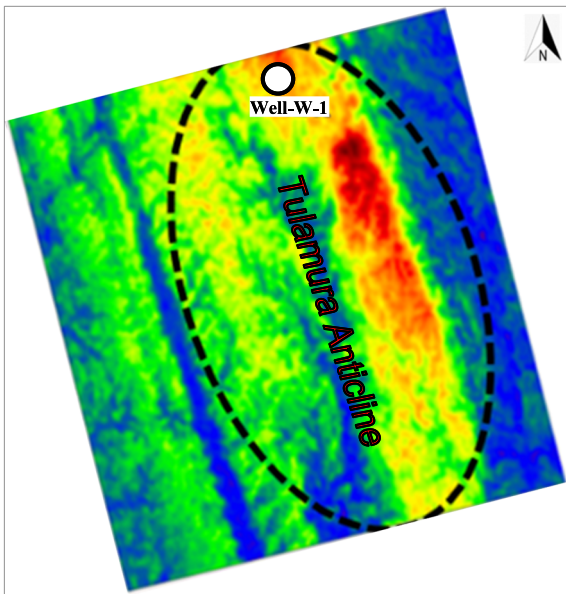


Figure 2. The DEM map shows the topographic variation in the study area. Red represents topographic high, and blue represents topographic low.

Moreover, the V_p/V_s ratio also discriminates between sand and shale facies based on their distinct magnitude response. Generally, channel features consist of porous sands that create more accommodation space for the concentration of hydrocarbon and mineralization fluids (Bhattacharjee *et al.* 2017). Therefore, porosity estimation is crucial to assess the sand quality and the fluids' holding capacity. The neural network-based tool allows additional inputs from the seismic and well-log data to generate the target outcomes (Hami-Eddine *et al.* 2009; Singh *et al.* 2016; Pandey *et al.* 2020; Dixit *et al.* 2020; Narayan *et al.* 2023a, b). The primary objective of the present study is to delineate the possible channel geometry within the Bhuban Formation in the Tulumura field and its characterization based on petrophysical properties derived using joint inversion and machine learning methods. This study in Tulumura anticline, Tripura, unveils a promising lead for hydrocarbon exploration. The flowchart for

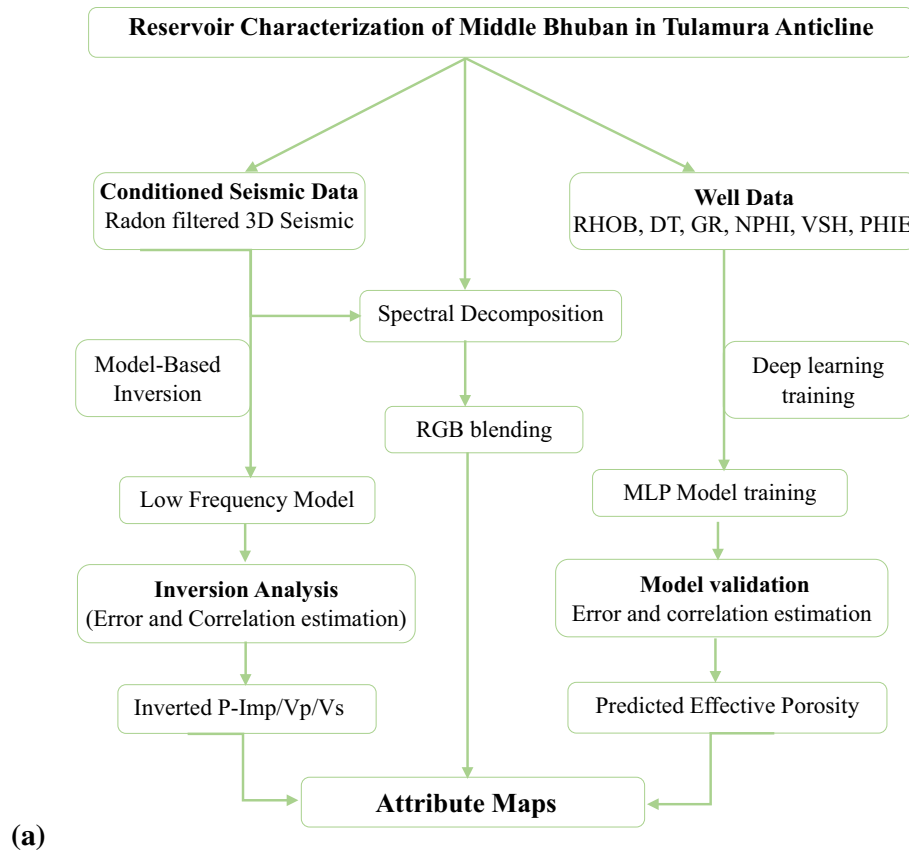


Figure 3a. Methodology flowchart for the delineation and reservoir characterization of Middle Bhuban in Tulumura anticline, Assam Basin.

delineation and reservoir characterization of the Bhuban Formation in Tulamura anticline, Assam Basin, is shown in figure 3(a).

2. Geology of the study area

2.1 Regional tectonics

The Assam and Assam Arakan Basin evolved due to rifting and drifting of the Indian plate towards the north and northeast after the Gondwanaland break up during the Cretaceous (Murty 1983; Naik *et al.* 2001; Narayan *et al.* 2023b, d). Indian subcontinent drifting caused Indian plate subduction below the Burmese plate. Oblique subduction of the Indian plate initiated the closing of the Neo-Tethys Ocean on the northeast and then gradually progressed southward. The westward migration of the prism complex extended into the Tripura–Cachar Fold Belt (TCFB) as the Neogene Accretionary Prism (Dasgupta and Nandy 1995). Initiation of structuration is considered to have occurred during the Mio-Pliocene, probably after the deposition of the Tipam Formation (Mohan and Pandey 1973). Detachment folding is the predominant mechanism of fold formation in the Tripura area. Several major anticlinal structures have been identified in Tripura through remote sensing studies and systematic geological mapping, and Tulamura anticline is among them.

2.2 Stratigraphy

The generalized litho-stratigraphy of the Tripura–Cachar area is shown in figure 3(b). A thick succession of argillaceous and arenaceous sequences represents the Neogene sediments of the Miocene Surma Group (Nandy *et al.* 1983). Surma Group is unconformably overlain by dominantly arenaceous Tipam Formation deposited in a fluvial environment. The Surma Group of sediments is further subdivided into Bhuban and Bokabil Formations. Bhuban Formation was further subdivided into three members: Lower Bhuban, Middle Bhuban, and Upper Bhuban, depending upon the relative abundance of coarser and finer clastics (Evans 1932). Bokabil Formation of Late Miocene to Early Pliocene age overlies the Bhuban Formations. Lower and Upper Bhuban Formations are more arenaceous than the Middle Bhuban, which is dominantly argillaceous, comprising mainly mudstone, shale, shale-siltstone alternation, and shale-sandstone alternation. The Surma Group of sedimentary succession lacks age-diagnostic fauna and marker horizons; hence, biostratigraphy control is minimal. During the Middle Eocene to Early Miocene, the collision of the Indian plate with the Burmese plate and Tibetan plate resulted in a major switch in sedimentation pattern over the Bengal Basin (Pal *et al.* 2016; Narayan *et al.* 2021, 2022a, b). The TCFB has undergone several stages of sedimentation. Surma Group sediments were deposited in a deltaic setting (Holtrop and Keizer 1970;

Age	Formation	Approx Thickness	Dominant Lithology
Early Pliocene	Tipam	720 m	Mainly arenaceous with shale and siltstone interlamination
Late Miocene	Bokabil	900m	Dominantly shale/claystone with few sandstone beds
Middle Miocene	Upper Bhuban	550m	Mainly sandstone with alternation of thick shale with siltstone
Early Miocene	Middle Bhuban	700m	Dominantly argillaceous sequence with siltstone and sandstone intercalations
	Lower Bhuban	1200m	Mainly arenaceous with siltstone interlamination and few thick shale sequences

(b)

Figure 3b. Stratigraphic chart of the Tripura–Cachar Fold Belt.

Johnson and Nur Alam 1991) with occasional marine transgressions (Seshavatham *et al.* 1998). Most of the sand facies in Tripura are heterogeneous and lenticular. The sedimentological studies indicate that the Middle Bhuban sediments were deposited in the delta front environment. In contrast, the Upper Bhuban sediments in the area are believed to be deposited under marginal marine in the mouth bar to distal bar regime (Dutta 1993) with fluctuating sea levels. Sand facies consisting of channels, distributary mouth bars, tidal bars and channel lobes are expected to occur under this depositional setup.

3. Data used

The 3D survey (south Tulamura anticline) covers an area of around 50 km² of pre-stack seismic data. The seismic data used for the study is the processed pre-stack time migration (PSTM) gathered in the time domain. It is found that the event is dipping at the far offset (figure 4a), which warrants gathering seismic data conditioning. To improve the quality of input seismic gathers, data conditioning through radon filtering was performed to remove the random noise. Subsequently, mild trim statics were applied for the event flattening. Figure 4(b) shows the seismic gather data quality improvement after conditioning. Further, well-to-seismic calibration was carried out to tie the formation tops marked at well with seismic reflectors (figure 4c). Three horizons (Upper, Middle and Lower Bhuban) have been mapped using the stacked seismic data. Figure 5(a) shows a representative seismic section showing the structural and stratigraphic configuration of the Tulamura anticline. Frequency bandwidth between 8 and 48 Hz was found in the zone of interest (figure 5b). The time structure map at the top of Middle Bhuban is depicted in figure 5(c). This two-way time structure map demonstrates the distinct anticlinal high signature bounded by the two longitudinal NNW–SSE trending thrust faults (figure 5c). The time range for the Middle Bhuban horizon varies from 1936 ms at anticline flanks to 569 ms at anticline crest. Faults are considered conduits and play a key role in fluid movement. Major faults with a substantial throw also restrict fluid movement and provide suitable entrapment conditions.

The only well (W-1) in the study area has a variety of recorded logs, viz., gamma-ray (GR), P- and S-waves (sonic wave velocity (DT) and shear wave velocity (DTSM)), density (RHOB),

resistivity and porosity throughout the Bhuban Formation. Depth matching between logs of a particular well is the first step for arriving at an accurate petrophysical evaluation. The well-log panel, comprising gamma-ray, density, resistivity, neutron porosity, P-impedance, Vp/Vs ratio, and effective porosity (PHIE), were studied to recognize the thickness of the sandstone facies from Middle Bhuban (2230–2340 ms). It is found that the identified sandstone facies were deposited in a fining upward sequence (figure 6a).

Well-based reservoir characterization was initially performed by cross-plotting the P-impedance *vs.* Vp/Vs ratio and P-impedance *vs.* effective porosity, colour-coded with litho-facies logs (figure 6b, c). It is found that the targeted sand facies correspond to the relatively low Vp/Vs ratio (1.6–1.8) and high effective porosity (10–20%) response with respect to shale and siltstone facies. On the other hand, it was also found that the sand, siltstone, and shale facies overlap in P-impedance response. Taking the lead from the above analysis, we attempted to delineate and characterize the sand facies using seismic-derived elastic and petrophysical properties.

4. Methods

4.1 Spectral decomposition and RGB blending

Spectral decomposition is also one of the most effective techniques for delineating channel geometry and its continuity (Chopra and Marfurt 2016). The wavelet transform technique known as the continuous wavelet transform (CWT) is extensively useful in the spectral decomposition of seismic data. Mathematically, the CWT technique is expressed as the inner product of the wavelet family $\psi_{\sigma,\tau}(t)$ with the signal $u(t)$.

$$S_w(\sigma, \tau) = \frac{1}{\sqrt{\sigma}} \int_{-\infty}^{\infty} u(t) \bar{\psi} \left(\frac{t - \tau}{\sigma} \right) dt \quad (1)$$

where $\bar{\psi}$ is the complex conjugate of ψ , and S_w is the time scale map used to extract the instantaneous frequency. τ is the time shift applied to the mother wavelet, and σ is the scale.

Spectral decomposition is the most effective technique for delineating channel geometry and its continuity (Chopra and Marfurt 2016). The PSTM stacked seismic data contains a frequency bandwidth of 8–48 Hz with a dominant frequency of 26 Hz (figure 5a, b). Considering this, we have

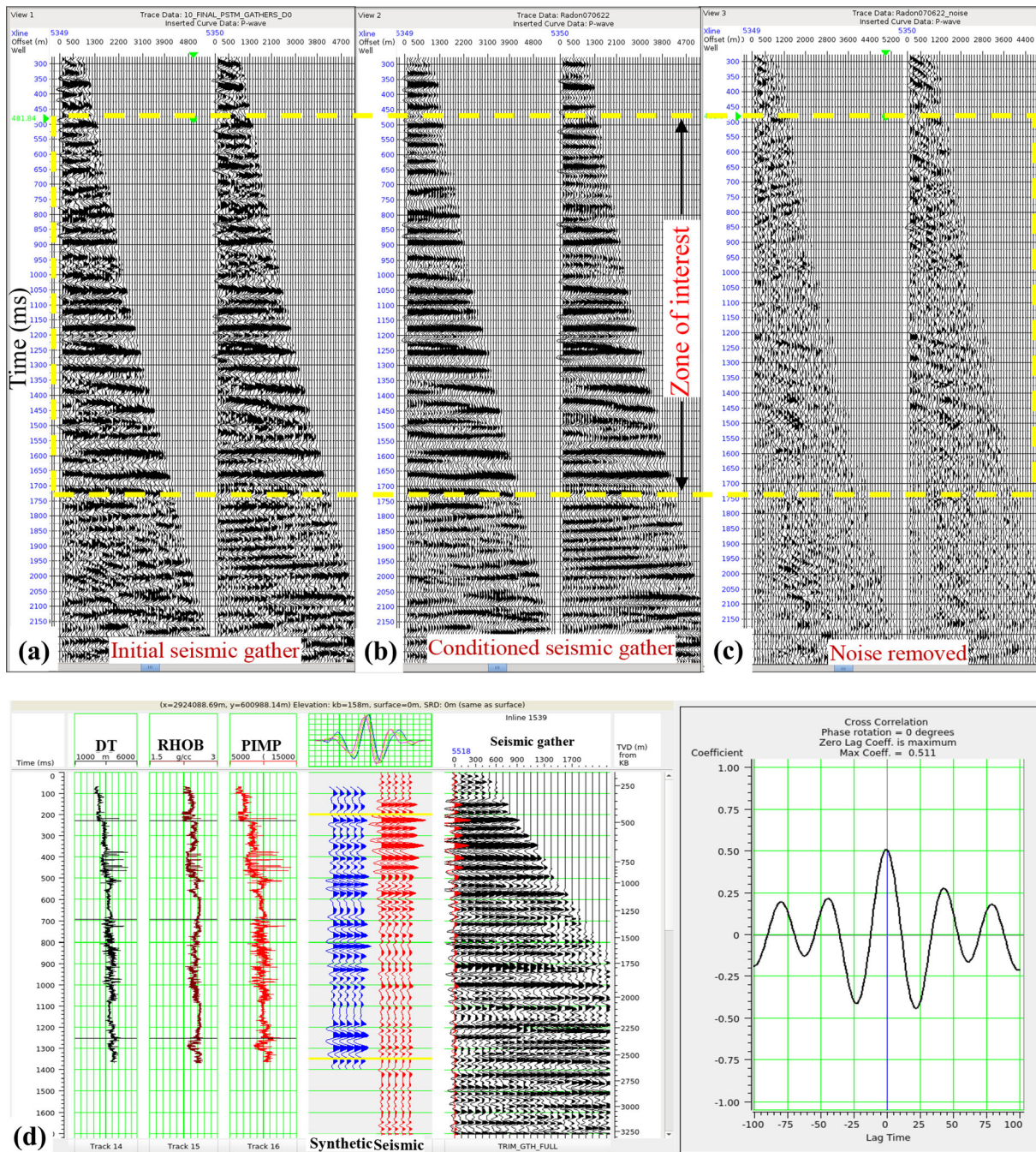


Figure 4. Seismic gather data. (a) Vintage processed seismic gather, (b) conditioned seismic gather and (c) noise. (d) Well to seismic tie using pre-stack seismic data for the zone of interest (marked yellow dotted box). A good correlation was achieved between the synthetic and the actual seismic.

generated iso-frequency volumes of 12, 20, 28 and 36 Hz. RGB (red-green-blue) blending of the spectrally decomposed (12, 20 and 28 Hz) seismic amplitude illuminates a southward trending channel geometry (figure 12a). Moreover, the identified channel feature must be characterized using advanced seismic attributes to ascertain the presence of good sand facies within the channel. The shale facies present in the surroundings of the

channel geometry will provide the lateral seal to restrict the fluid flow that may contain hydrocarbons.

4.2 Pre-stack seismic inversion and P-impedance and V_p/V_s ratio estimation

Several authors have discussed pre-stack seismic inversion methods to obtain reliable estimates of

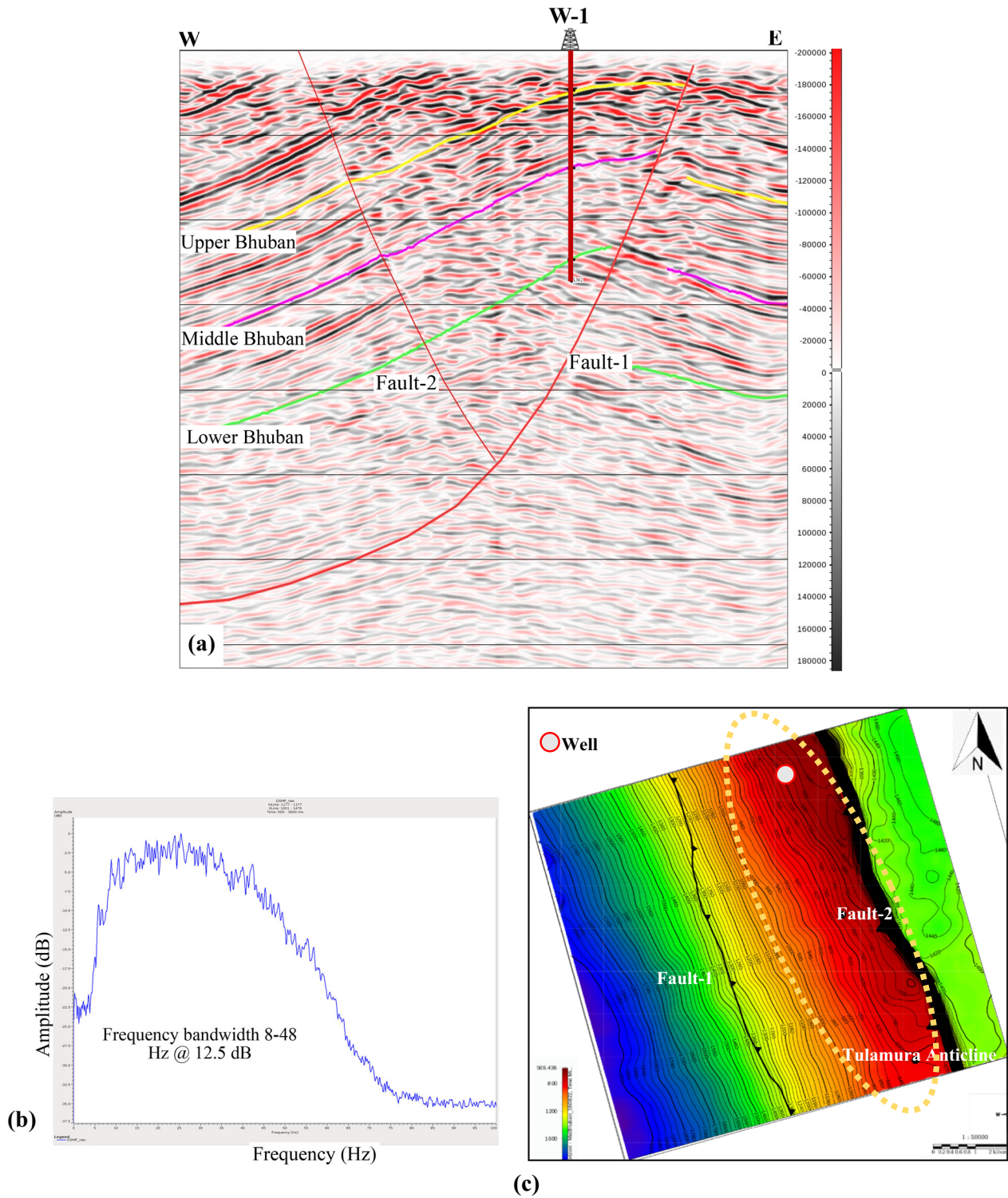


Figure 5. (a) The inverse seismic section passing through well W-1 demonstrates the formation tops and major and minor faults. (b) Frequency bandwidth between 8–48 Hz was found in the zone of interest. (c) The structure map at the Middle Bhuban top shows the Tulamura anticline and structure-bounding thrust faults.

P-impedance, S-impedance, density and V_p/V_s ratio (Simmons and Backus 1996; Buland and Omre 2003; Hampson *et al.* 2005; Russel *et al.* 2006; Zhang *et al.* 2011; Xiao *et al.* 2020; Sun *et al.* 2022).

This research used model-based inversion to estimate the acoustic impedance and V_p/V_s ratio volumes. The discussion about the detailed methodology for estimating the P-impedance and

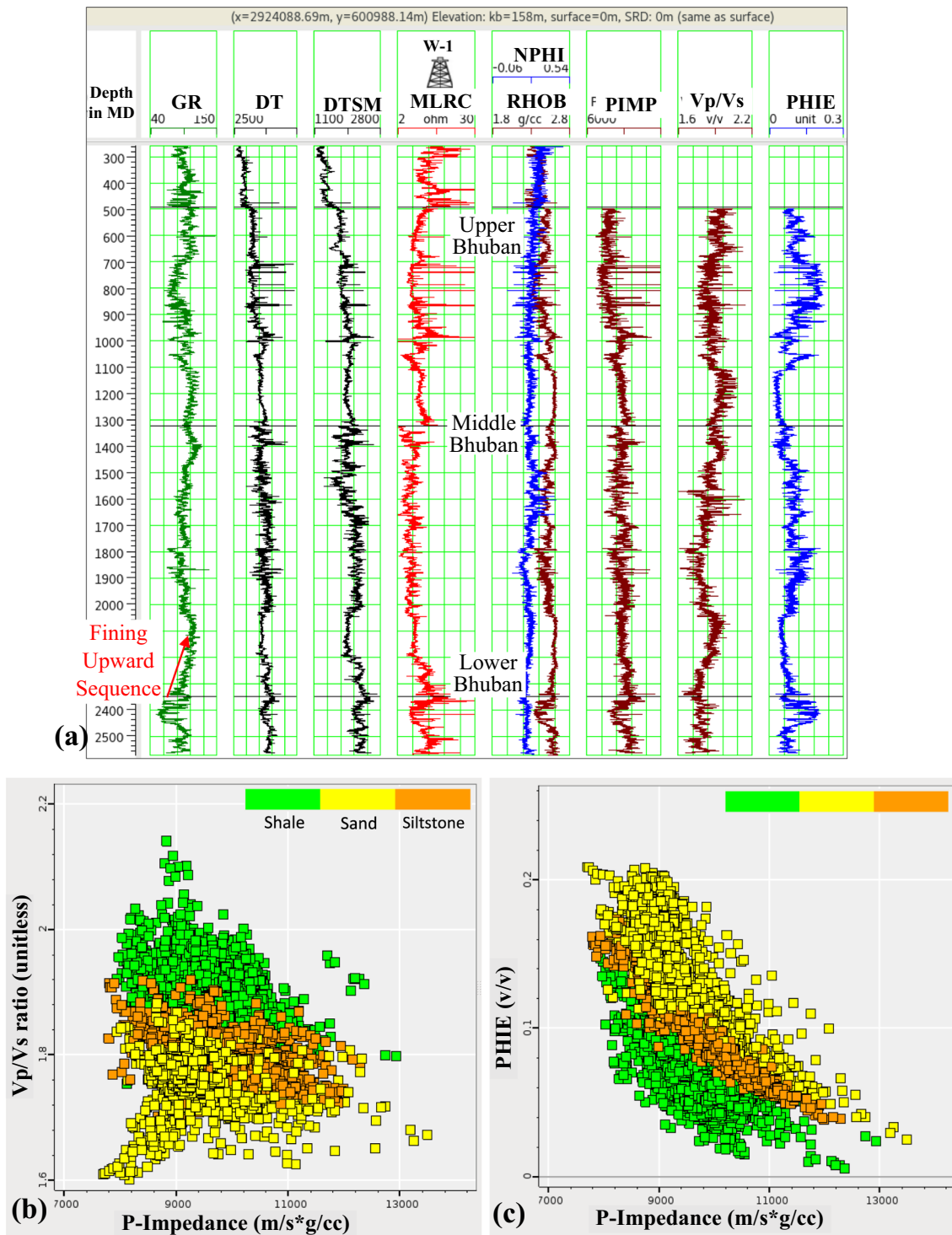


Figure 6. (a) Well-log panel showing various log signatures. Gamma-ray log interpretation indicates thick sand facies deposited in a fining upward sequence at the Middle Bhuban base. (b) Well-based cross-plot between P-impedance vs. Vp/Vs ratio and (c) P-impedance vs. effective porosity (PHIE), indicating the characteristics of the sand (yellow), siltstone (brown) and shale facies (green).

Vp/Vs ratio is beyond the scope of this paper. This study found a suitable wavelet time length of 160 ms, requiring a seismic window of 500 to 600 ms for reliable inversion. Including shallower seismic responses in wavelet estimation captures the

influence of lithologies encountered by seismic rays. However, readers seeking detailed information regarding the pre-stack inversion process may refer to the research articles by Fatti *et al.* (1994), Hampson *et al.* (2005) and Russel *et al.* (2006). We

adopted the workflow to invert the 3D pre-stack seismic data shown in figure 7.

This study carried out pre-stack seismic inversion to generate P-impedance and Vp/Vs ratio volumes. The accuracy of the inverted results was evaluated through cross-plot analysis and comparison with log signatures at the well point (figure 8a–c). A linear relationship with good correlation (P-impedance: 87.8% and Vp/Vs ratio: 93.1%) was found between the inverted and actual logs with errors of nearly $337 \text{ m/s} * \text{ gm/cm}^3$ and 0.23, respectively. The estimated P-impedance and Vp/Vs ratio inline sections passing through well (W-1) overlaid with log P-impedance validate the inverted outcomes (figure 9a, b). The target sand facies are characterized by relatively moderate P-impedance ($9800\text{--}10600 \text{ m/s} * \text{ gm/cm}^3$) and low Vp/Vs ratio (1.68–1.76), as shown in figure 9(a, b). It is also found that the Vp/Vs ratio and P-impedance attributes efficiently discriminate between the sand and shale facies.

4.3 Multilayer perceptron (MLP) modelling and effective porosity prediction

The perceptron is a widely used neural network approach for binary problem-solving. It utilizes activation functions that exhibit monotonically increasing behaviours (Van der Baan and Jutten 2000; Dixit and Mandal 2020; Narayan *et al.* 2023a, c). As a fundamental model, the perceptron

serves as a mathematical representation of how the human mind operates. It receives input information from the input layer (seismic attributes), applies weights to the inputs, calculates their sum, passes the result through an activation function, and generates an output in the output layer. The network’s performance is assessed based on its number of hidden layers. Insufficient hidden layers can lead to poor performance. In contrast, excessive hidden layers may cause the network to merely memorize the training data and fail when presented with unknown datasets (McCormack 1991).

To create an improved multilayer perceptron (MLP) model, adjustments are required to the number of neurons in the hidden layers, in addition to appropriately updating the weights based on the complexity of the problem at hand (Van der Baan and Jutten 2000; Hami-Eddine *et al.* 2009). Assuming the input vectors as x_1, x_2, \dots, x_n , and the corresponding weights as w_1, w_2, \dots, w_n , the output of a perceptron can be represented by the following equation:

$$y = \sum_{i=1}^n w_i x_i + bias. \tag{2}$$

It can also be written as,

$$y = w^t x + bias. \tag{3}$$

The difference between the expected and actual output is minimized through iterative

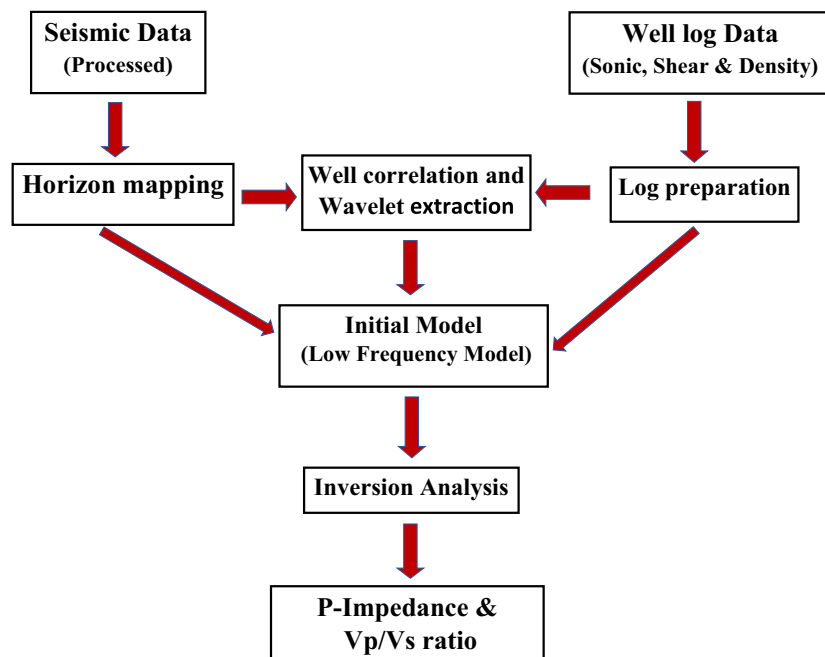


Figure 7. Workflow adopted for the inversion of pre-stack seismic data.

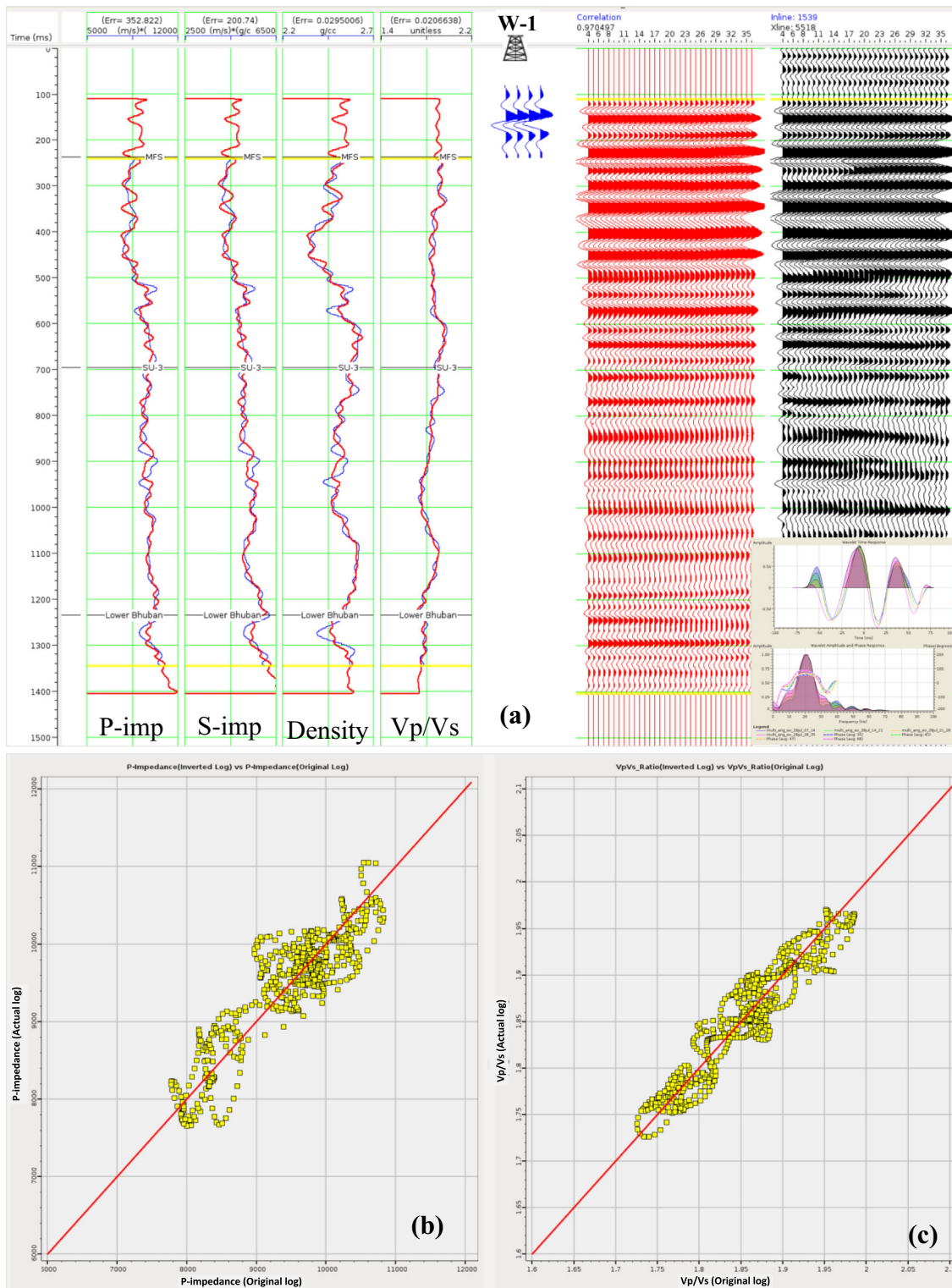


Figure 8. (a) Inversion analysis using single trace seismic attribute showing good correlation between original and inverted impedance/(Vp/Vs) ratio and lower synthetic error at well W-1. The wavelet used in this inversion process is shown in the inset. (b, c) Cross-plot results indicate a linear relationship between the inverted P-impedance/(Vp/Vs) ratio and the actual P-impedance/(Vp/Vs) ratio.

back-propagation learning (Singh *et al.* 2016; Dixit and Mandal 2020). Seismic attributes (listed in table 1) involve diverse mathematical transformations

of seismic trace data, enhancing predictive capabilities and pattern recognition through the nonlinear responses of attributes during MLP

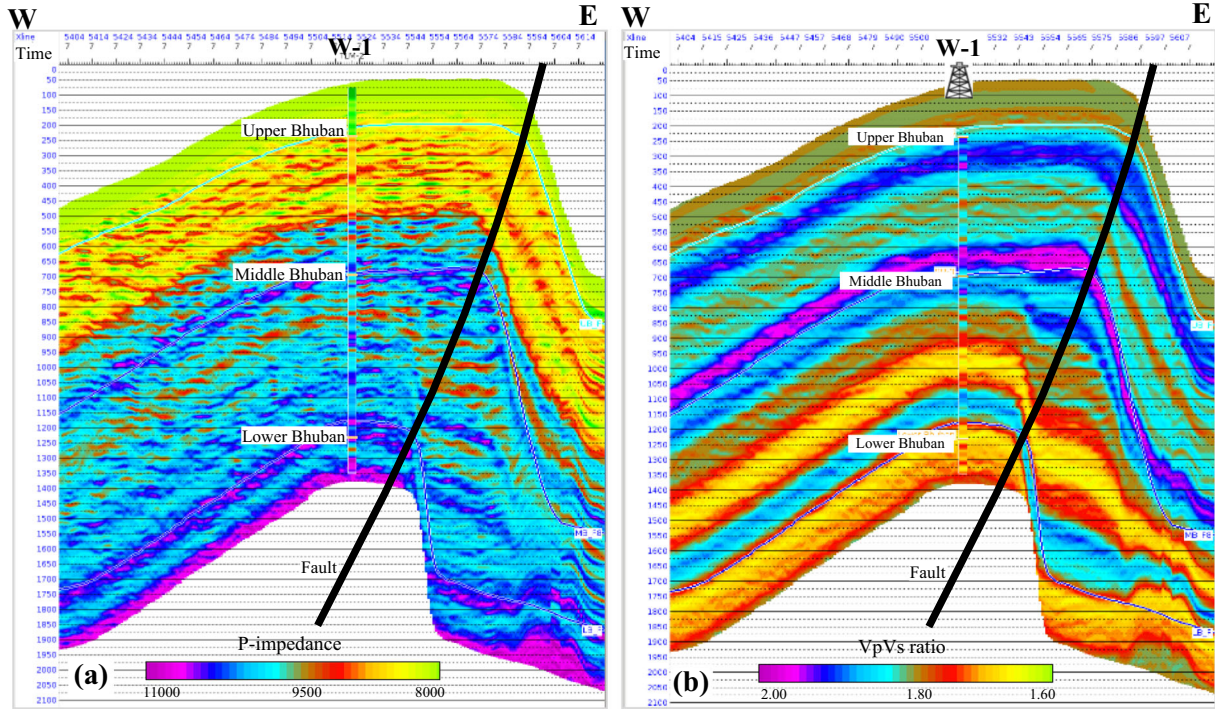


Figure 9. Inline passing through well W-1 extracted from (a) P-impedance and (b) Vp/Vs ratio are shown here. The log impedance and Vp/Vs ratio strips overlaid on the corresponding inverted impedance and Vp/Vs ratio show an excellent match.

Table 1. Post-stack seismic derived attributes used for neural network training and validation.

Sl. no.	Different attributes
1	Acoustic Impedance (Inverted P-imp)
2	Instantaneous Average Amplitude (IAA)
3	Amplitude Weightage Frequency (AWF)
4	Average Frequency (AF)
5	Dominant Frequency (DF)
6	Amplitude Envelope (AE)
7	Derivative (DER)
8	Amplitude Weightage Cosine Phase (AWCP)
9	Second Derivative (SD)
10	Apparent Polarity (AP)
11	Dominant Instantaneous Amplitude (DIA)
12	Raw Seismic (DSMF)
13	Quadrature Trace (QT)
14	Integrate (INT)
15	Amplitude Weightage Phase (AWP)
16	Cosine Instantaneous Phase (CIP)
17	Instantaneous Frequency (IF)
18	Instantaneous Phase (IP)

model training (Hampson *et al.* 2005). Before the combination, all input data were randomized and standardized to eliminate any potential bias. The model is trained using 75% of the input data, while the remaining 25% is left out for validation

(testing) purposes. Sensitivity analyses identified vital features in effective porosity prediction and found that each attribute significantly contributes to property prediction. Among all input attributes, we found that the P-imp attribute has more feature importance than the other attributes (figure 10a). The correlation coefficient between initial and predicted PHIE values was 94.1% (figure 10b). The trained model achieved the lower mean absolute error (MAE) (~ 0.015) and average loss (~ 0.005) on the test data (figure 10c and d). MAE measures how close the predicted values are to the actual values on average. A lower MAE indicates better accuracy, representing a smaller average deviation from the actual values. The high correlation coefficient and reduced errors demonstrate the model’s efficacy in predicting PHIE volume. After getting an error below an acceptable threshold, the predicted PHIE was accepted, and the PHIE volume was generated. The predicted PHIE values closely matched the overlaid log PHIE strip. The PHIE measures the interconnected pore spaces in the sedimentary rock. The PHIE efficiently discriminates between the sand facies (relatively high PHIE) and shale facies (very low PHIE) and signifies the quality of sand facies. We found a high-PHIE (8–13%) response for the target sand zone (figure 11).

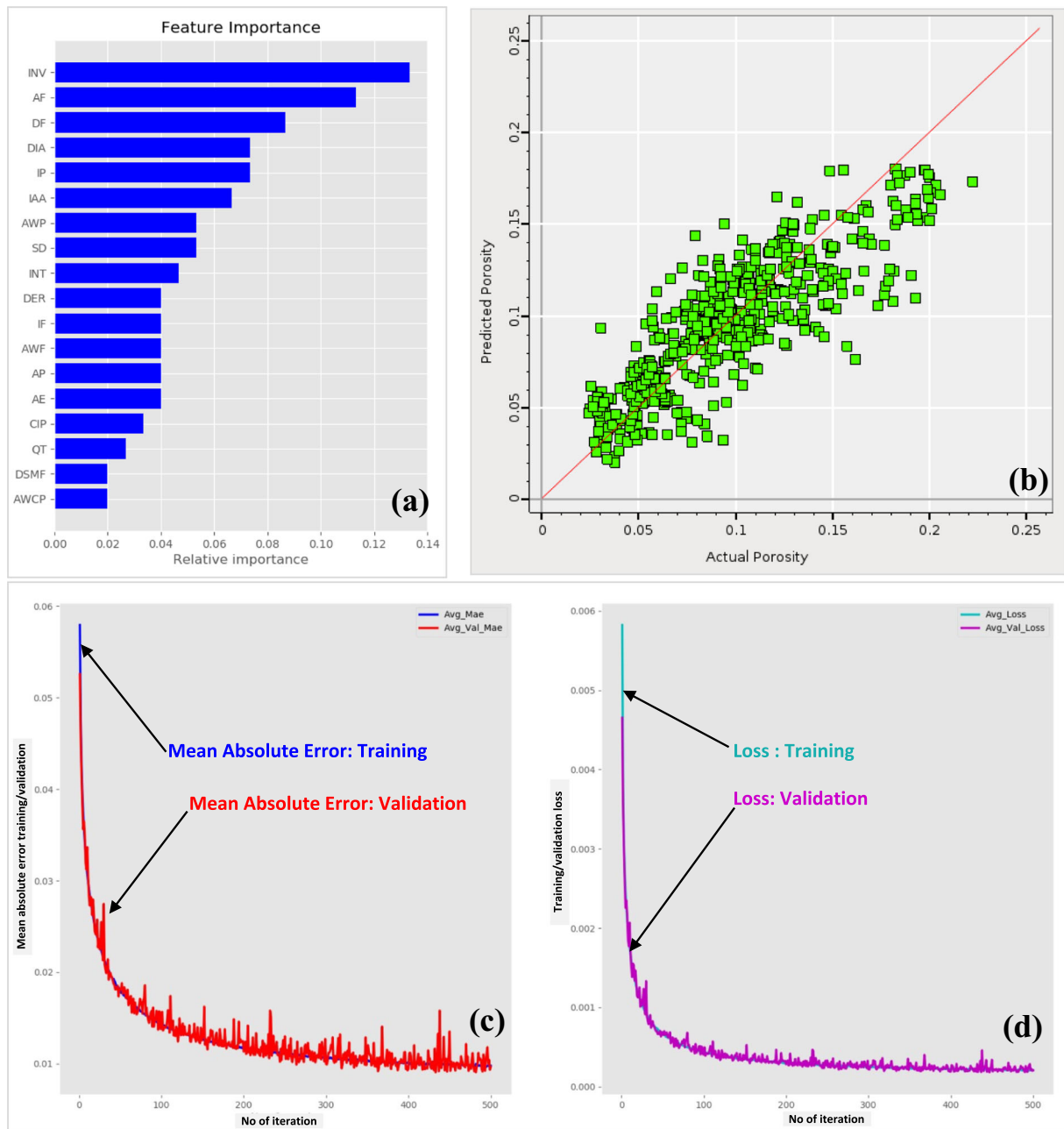


Figure 10. (a) Relative feature importance found for different attributes used in machine learning modelling. (b) Cross-plot result indicating a linear relationship between the actual and predicted effective porosity with high correlation. (c) Lower training/validation mean absolute error. (d) Lower training/validation loss values obtained at 500 iterations indicate that the porosity volume was estimated with high accuracy.

5. Results and discussions

We identified thick sandstone facies (~60 m) deposited in channel geometry at the Middle Bhuban base encountered in the well W-1. State-of-the-art geophysical and machine learning techniques were utilized to pursue this lead in the Tulamura field, combining well-log and seismic data. High-resolution 3D seismic data provides broader coverage with enhanced continuous

subsurface imaging capability. Subsequently, it can be best utilized in mapping various litho-stratigraphic layers and in subsurface facies characterization from the surrounding rocks.

In the Tripura–Cachar Fold Belt, India, most channel features have been observed along the NNE–SSW direction with SSW flow (Kumar *et al.* 2016; Bhattacharjee *et al.* 2017). The sandstone facies within the channel geometry were mainly coarse to medium-grained, arkosic, and reducing.

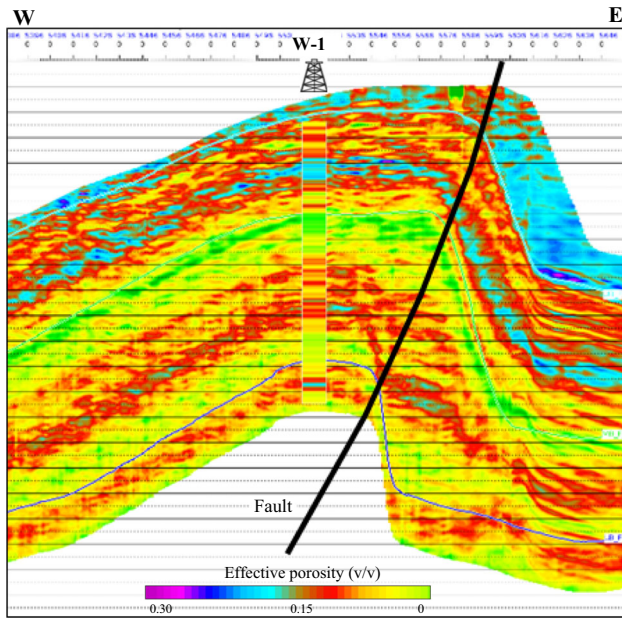


Figure 11. Inline passing through well W-1 extracted from the effective porosity is shown here. The log porosity strip overlaid on the predicted porosity shows a good match.

The studies reveal that the sandstone facies were deposited in fan, braided rivers of typical proximal facies with fining upward sequences (Kumar *et al.* 2016). We studied 3D seismic and well-log data to delineate the structural architecture and characterize the stratigraphic sequences in the Tulamura field. Gamma-ray log study suggests that the porous sand facies were deposited in a fining upward sequence (figure 6a). The overlying shale layer (impermeable) may act as the top seal for the hydrocarbon accumulations. The correlation between the sand facies and the elastic and petrophysical properties (P-impedance, V_p/V_s ratio and effective porosity) was established through cross-plot analysis at the well point (figure 6b, c). The results suggest that the ore-containing sandstone facies pose relatively moderate P-impedance, low- V_p/V_s ratio and highly effective porosity signatures with respect to surroundings. The structural mapping shows two NNW–SSE trending thrust faults bound the Tulamura anticline and may provide suitable structural entrapment conditions (particularly eastward fault) for fluid accumulation (figure 5b).

Seismic-derived attributes were analyzed to delineate and characterize the possible dispersal pattern of the identified sandstone facies in the study area. RGB blend spectrally decomposed seismic response indicates an almost southward trending channel geometry almost parallel to the

ENE–SSW trending major fault (figure 12a). The varied tuning frequencies observed across different segments of the channel geometry signify the presence of lithological heterogeneities within its structure. The type and nature of the facies from the channel geometry were further characterized based on P-impedance, V_p/V_s ratio and effective porosity responses (figure 12b–d) (Wood *et al.* 2012). The zones within the channel geometry indicate relatively moderate P-impedance (figure 12b), low V_p/V_s ratio (figure 12c) and high effective porosity (figure 12d), indicating good porous sands (average effective porosity $\sim 9\%$) for hydrocarbon accumulations in Tulamura field, Tripura, India. Our analysis reveals that the predominant sedimentary fill within the channel geometry consists of sand facies.

Nonetheless, transitions in litho-facies, potentially from clean sand to silt or shaly sand, are apparent, corroborating the findings derived from RGB blending. Dasgupta and Nandy (1995) suggested that the Bhuban Formation sediments were deposited in the delta front environment to the under marginal marine in the mouth bar to distal bar regime with fluctuating sea level. The levee part is argillaceous. These shale facies between channel geometry and the NNE–SSW trending major fault may provide good lateral entrapment conditions for fluid accumulations. The present study thoroughly discusses the structural and stratigraphic aspects of hydrocarbon exploration in the study area. Some studies have been conducted in the Penobscot field; Nova Scotia poses complex geological structures, limited well log data and moderate seismic data quality. These studies provide an efficient and reliable geological model in petroleum exploration (Narayan *et al.* 2023a, c).

6. Conclusions

In this study, we applied machine learning and state-of-the-art geophysical tools on 3D seismic data to delineate and characterize the geologic features containing hydrocarbon in the Tripura–Cachar Fold Belt, India. The spectral decomposition result efficiently delineates the almost southward trending channel geometry. The petrophysical properties (P-impedance, V_p/V_s ratio and effective porosity) estimated with high precision have been utilized to delineate and characterize the channel in-fill litho-facies. Based on relatively moderate P-impedance ($9800\text{--}10600 \text{ m/s} * \text{ gm/cm}^3$),

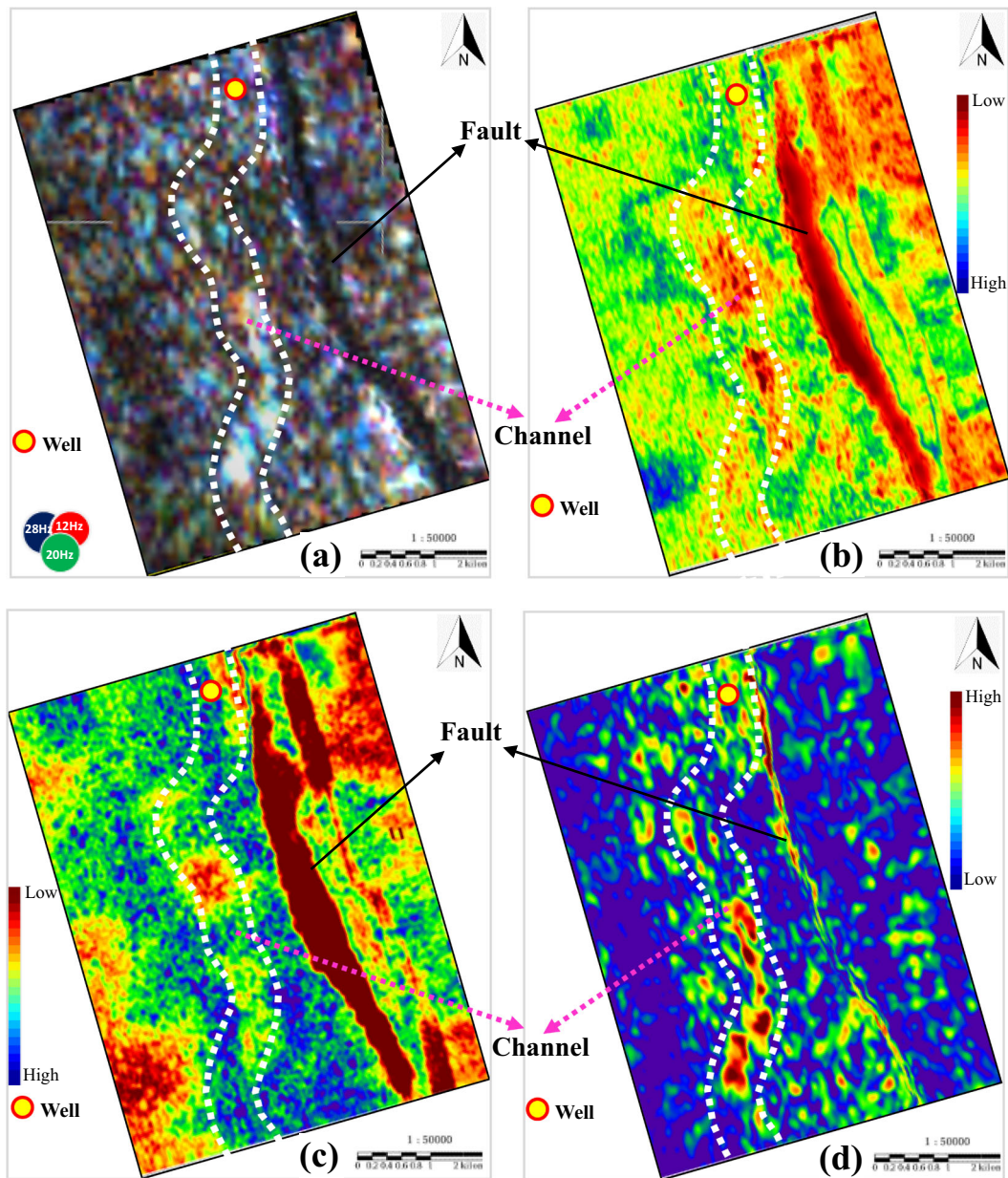


Figure 12. Attribute maps were generated for the (a) RGB blend spectral decomposed seismic, (b) P-impedance, (c) V_p/V_s ratio, and (d) effective porosity.

low V_p/V_s ratio (1.68–1.76) and high effective porosity (8–13%), it is found that the channel geometry is mainly filled with porous sand facies deposited in fining upward sequences. These porous sand facies could be a favourable reservoir for hydrocarbon exploration from Middle Bhuban deposits in the Tulamura field in Tripura. The impermeable shale facies at the sand top and between the channel geometry and NNE–SSW trending fault will provide a suitable stratigraphic entrapment for hydrocarbon fluids. The present

study estimates the extension, orientation, and spatial occurrences of porous sand reservoir facies, and the sand facies with good porosity are the favourable zones possibly containing hydrocarbon. The present study also highlights the importance of machine learning and the utilization of geophysical tools in hydrocarbon exploration to get a clearer image of the subsurface. However, seismic data quality and limited well data are the main problems in the Tulamura field that need to be addressed.

Acknowledgements

The authors are grateful to Director, ONGC Limited, for permission to publish this work. The authors are also thankful to the Editorial Team, the Journal of Earth System Science and two anonymous reviewers for their constructive review and thoughtful suggestions towards the improvement of this work.

Author statement

PK: Conceptualization, written original draft, data curation, methodology, analysis and investigation; SN: Conceptualization, formal analysis, review and edition and correspondence; RM: Methodology, analysis, literature review and result validation; BP: Review and supervision.

References

- Bhattacharjee P, Rengarajan M, Srivastava S K, Hamilton S and Mohanty R 2017 Paleochannel-controlled depositional features of the Cretaceous Lower Mahadek Uranium mineralization in Umthongkut area, West Khasi Hills, Meghalaya; *J. Geol. Soc. India* **90** 175–182.
- Biswas A, Mandal A, Sharma S P and Mohanty W K 2014 Integrating apparent conductance in resistivity sounding to constrain 2D gravity modelling for subsurface structure associated with uranium mineralization across South Purulia Shear Zone; *Int. J. Geophys.*, <https://doi.org/10.1155/2014/691521>.
- Buland A and Omre H 2003 Bayesian linearized AVO inversion; *Geophysics* **68** 185–198.
- Chopra S and Marfurt K J 2016 Spectral decomposition and spectral balancing of seismic data; *The Lead. Edge* **35** 176–179.
- Darijani M, Farquharson C G and Lelievre P G 2019 Clustering and constrained inversion of seismic refraction and gravity data for overburden stripping: Application to uranium exploration in the Athabasca Basin, Canada; *Geophysics* **85**(4) B133–B146.
- Dasgupta S and Nandy D R 1995 Geological framework of the Indo-Burmese convergent margin with special reference to ophiolite emplacement; *Indian J. Geol.* **67** 110–125.
- Dutta S K 1993 *Geology of north-east India*; Omsons Publications, New Delhi.
- Evans P 1932 Tertiary succession in Assam; *Trans. Min. Geol. Inst., India* **27** 155.
- Fatti J L, Smith G C, Vail P J, Strauss P J and Levitt P R 1994 Detection of gas in sandstone reservoirs using AVO analysis: A 3-D seismic case history using the Geostack technique; *Geophysics* **59** 1362–1376.
- Hami-Eddine K, Klein P and Richard L 2009 Well facies-based supervised classification of pre-stack seismic: Application to a turbidite field; *79th Annual Int. Meeting. SEG. Expanded Abstracts*. pp. 1885–1889.
- Hampson D, Russell B and Bankhead B 2005 Simultaneous inversion of pre-stack seismic data; In: *Society of Exploration Geophysicists – 75th SEG International Exposition and Annual Meeting, SEG-2005*; Soc. of Expl. Geophys., Houston, TX, USA, pp. 1633–1637.
- Holtrop J F and Keizer J 1970 Some aspects of stratigraphy and correlation of the Surma Basin wells, East Pakistan; *ESCAPE Mineral Res. Devel. Series* **36** 143–154.
- Johnson S Y and Nur Alam M 1991 Sedimentation and tectonics of the Sylhet trough, Bangladesh; *Geol. Soc. America Bull.* **103** 1513–1527, <https://doi.org/10.1130/0016-7606>.
- Kumar R, Das B, Chatterjee R and Sain K 2016 A methodology of porosity estimation from inversion of post-stack seismic data; *J. Nat. Gas Sci. Eng.* **28** 356–364.
- Latimer R B, Davidson R and Van Riel P 2000 An interpreter's guide to understanding and working with seismic derived acoustic impedance data; *The Lead. Edge* **19**(3) 242.
- Mohan M and Pandey J 1973 Early Paleogene eco-stratigraphy of Upper Assam; *Bull. Ind. Geol. Assoc.* **6**(1) 47–62.
- Murty K N 1983 Geology and hydrocarbon prospects of Assam Shelf-Recent advances and present status; *Petrol. Asia J.* **1** 1–14.
- Naik G C *et al.* 2001 Sequence stratigraphy and petroleum systems of Assam Shelf; *unpublished report, BSD, KDMIPE, ONGC*.
- Nandy D R, Dasgupta S, Sarkar K and Ganguly A 1983 Tectonic evolution of Tripura-Mizoram Fold Belt, Surma Basin, Northeast India; *Quart. J. Geol. Min. Met. Soc. India* **55**(4) 186–194.
- Narayan S, Kumar U, Pal S K and Sahoo S D 2021 New insights into the structural and tectonic settings of the Bay of Bengal using high-resolution earth gravity model data; *Acta Geophys.*, <https://doi.org/10.1007/s11600-021-00657-8>.
- Narayan S, Sahoo S D, Pal S K and Kumar U 2022a Comparative evaluation of five global gravity models over a part of the Bay of Bengal; *Adv. Space Res.*, <https://doi.org/10.1016/j.asr.2022.11.002>.
- Narayan S, Mohan A, Kumar V and Acharya A 2022b Reservoir characterization Kopili sands using model-based impedance inversion and multilayer perceptron neural network in Lakwa Oilfield, Assam Basin, India; *Geohorizon* **27**(2) 101–117.
- Narayan S, Sahoo S D, Kar S, Pal S K and Kangsabanik S 2023a Improved reservoir characterization by means of supervised machine learning and model-based seismic impedance inversion in the Penobscot field, Scotian Basin; *Energy Geos.* 100180, <https://doi.org/10.3389/feart.2023.1150954>.
- Narayan S, Singh R, Mohan A, Vivek K, Acharya P and Pal S K 2023b Delineation of thin and discrete sand reservoir facies from shale-dominated Kopili Formation (Middle to Late Eocene) using the post-stack seismic inversion and neural network algorithm: A case study from Assam Basin, India; *J. Earth Syst. Sci.* **132** 81.
- Narayan S, Konka S, Chandra A, Abdelrahman K, András P and Eldosouky A M 2023c Accuracy assessment of various supervised machine learning algorithms in litho-facies classification from seismic data in the Penobscot field, Scotian Basin; *Front. Earth Sci.*, <https://doi.org/10.3389/feart.2023.1150954>.

- Narayan S, Saho S D and Pal S K *et al.* 2023d Integrated geophysical and petrophysical characterisation of Upper Jurassic carbonate reservoirs from Penobscot field, Nova-Scotia: A case study; *Mar. Geophys. Res.* **44** 23, <https://doi.org/10.1007/s11001-023-09533-0>.
- Pal S K, Narayan S, Majumdar T J and Kumar U 2016 Structural mapping over the 85°E ridge surroundings using EIGEN6C4 high-resolution global combined gravity field model: An integrated approach; *Mar. Geophys. Res.* **37** 159–184, <https://doi.org/10.1007/s11001-016-9274-3>.
- Pandey A K, Chatterjee R and Choudhury B 2020 Application of neural network modelling for classifying hydrocarbon bearing zone, water-bearing zone and shale with estimation of petrophysical parameters in Cauvery basin, India; *J. Earth Syst. Sci.* **129** 33, <https://doi.org/10.1007/s12040-019-1285-4>.
- Russell B, Hampson D and Bankhead B 2006 An inversion primer; *CSEG Rec.* **31** 96–103.
- Seshavataram B T V, Nandi P K and Choudhury S 1998 Petroleum geology of Cachar fold belt; *Proc. Reg. Sem. Dev. Geol. Res. in N.E. India, Gauhati University*, pp. 327–348.
- Simmons J L and Backus M M 1996 Waveform-based AVO inversion and AVO prediction-error; *Geophysics* **61** 1575–1588.
- Sun S, Luanxiao Zhao, Huaizhen Chen, Zhiliang H and Jianhua Geng 2022 Pre-stack seismic inversion for elastic parameters using model-data-driven generative adversarial networks; *Geophysics* **88**(2), <https://doi.org/10.1190/GEO2022-0314.1>.
- Wood G, O'Dowd C, Cosma C and Enescu N 2012 An interpretation of surface and borehole seismic surveys for mine planning at the Millennium uranium deposit, northern Saskatchewan, Canada; *Geophysics* **77**(5) WC203–WC212.
- Xiao S, Ba J, Guo Q, Carcione J M, Zhang L and Luo C 2020 Seismic pre-stack AVA inversion scheme based on lithology constraints; *J. Geophys. Eng.* **17**(3) 411–428.
- Zhang Y Y, Sun Z D, and Yang H J *et al.* 2011 Pre-stack inversion for caved carbonate reservoir prediction: A case study from Tarim Basin; *China. Pet. Sci.* **8**(4) 415–421.

Springer Nature or its licensor (e.g. a society or other partner) holds exclusive rights to this article under a publishing agreement with the author(s) or other rightsholder(s); author self-archiving of the accepted manuscript version of this article is solely governed by the terms of such publishing agreement and applicable law.

Corresponding editor: BAPPA MUKHERJEE